Journal of Alloys and Compounds 660 (2016) 231–234

Contents lists available at ScienceDirect

Journal of Alloys and Compounds

journal homepage: http://www.elsevier.com/locate/jalcom

High-performance $Ba(Zr_{0.1}Ce_{0.7}Y_{0.2})O_{3-\delta}$ asymmetrical ceramic membrane with external short circuit for hydrogen separation

Zhiwen Zhu [a], Jie Hou [b], Wei He [b], Wei Liu [b, *]

[a] Key Laboratory of Processing and Testing Technology of Glass & Functional Ceramics of Shandong Province, School of Materials Science and Engineering, Qilu University of Technology, Jinan, Shandong 250353, China
[b] CAS Key Laboratory of Materials for Energy Conversion & Collaborative Innovation Center of Suzhou Nano Science and Technology, University of Science and Technology of China, Hefei, Anhui 230026, China

ARTICLE INFO

Article history:
Received 28 July 2015
Received in revised form
6 October 2015
Accepted 10 November 2015
Available online xxx

Keywords:
$Ba(Zr_{0.1}Ce_{0.7}Y_{0.2})O_{3-\delta}$
Proton conductor
Asymmetric membrane
Hydrogen separation

ABSTRACT

$Ba(Zr_{0.1}Ce_{0.7}Y_{0.2})O_{3-\delta}$ asymmetric ceramic membrane with external short circuit (ESC asymmetrical membrane) was developed for further improving hydrogen separation efficiency. Hydrogen permeation flux(JH_2) of ESC asymmetrical membrane is higher than those of traditional Ni–$Ba(Zr_{0.1}Ce_{0.7}Y_{0.2})O_{3-\delta}$ membranes, e.g., 1.71×10^{-7} mol cm^{-2} s^{-1} for ESC asymmetrical membrane while 1.37×10^{-8} mol cm^{-2} s^{-1} for Ni-BZCY asymmetric membrane at 900 °C [11]. However, the activation energy of hydrogen permeation is higher for ESC asymmetrical membrane. Hydrogen fluxes of ESC asymmetrical membrane increase with the rising of temperature and hydrogen partial pressure gradient across both sides of membrane. The linear relationship between JH_2 and $\ln(p'H_2/p''H_2)$ indicates that hydrogen permeation occurs via the ambipolar diffusion of proton and electron in ESC asymmetrical membrane and is controlled by the bulk diffusion of proton. The stability testing in CO_2-containing atmosphere indicated that hydrogen permeation output remained unchanged in 3%CO_2 feed gas but a pronounced decline of 8% was observed after 50-h operation in 20% CO_2 feed gas.

1. Introduction

So far, the hydrogen separation membranes consisted of nickel and barium cerate possess undoubtedly the highest permeation performance among all kinds of membranes based on the high-temperature proton conductors [1–5]. However, its hydrogen permeation efficient is still lower than that of the practical application and limits the further development. In recent years, the efforts on membrane components, powder synthesis and surface modification etc. have been put into improvement of permeation performance and achieved some positive results. Yang et al. investigated the effect of nickel content in Ni–$BaCe_{0.9}Y_{0.1}O_{3-\delta}$ membrane on permeation flux and the results indicated that the membrane containing 30vol.% Ni has the best performance [6]. Yan et al. fabricated Ni–$BaZr_{0.1}Ce_{0.7}Y_{0.2}O_{3-\delta}$(BZCY) membranes using characteristic powders which were synthesized by a packing method, and hydrogen permeation measurement indicated a 18% increase at 900 °C [7]. Zhang et al. modified the surface of Ni–$BaCe_{0.8}Y_{0.2}O_{3-\delta}$ membrane using metal Pd, and therefore reduced the interface polarization and increased permeability [8].

In order to further increase hydrogen permeation output of Ni-BZCY composite membrane, optimization of membrane configuration is one way of overcoming problem. The Ni-BZCY composite membrane with symmetric structure (Fig. 1a) has often been adopted in many pervious studies on membrane permeation properties. Song et al. reported that the permeation flux and membrane thickness dependence of the Ni–$BaCe_{0.8}Y_{0.2}O_{3-\delta}$ membranes in thickness range of 0.08–1.16 mm, which indicated that the bulk diffusion is the rate limiting step in investigated thickness range [9]. According to the Wagner equation, when the bulk diffusion is the rate-limiting step the hydrogen permeation fluxes across membranes are inversely proportional to the thickness [10]. Hence, development of the asymmetrical Ni-BZCY membrane depicted in Fig. 1b is indispensable, which could efficiently decrease membrane thickness and then increase hydrogen permeation flux. In our previous study, an asymmetrical Ni-BZCY membrane with 30 μm-thickness dense layer was prepared, which displayed the high hydrogen permeation flux of 2.4×10^{-7} mol cm^{-2} s^{-1} using humidified 80%H_2/N_2 as feed gas and dry high purity argon as sweep gas [11]. For Ni-BZCY cermet

* Corresponding author.
E-mail address: wliu@ustc.edu.cn (W. Liu).

http://dx.doi.org/10.1016/j.jallcom.2015.11.065
0925-8388/

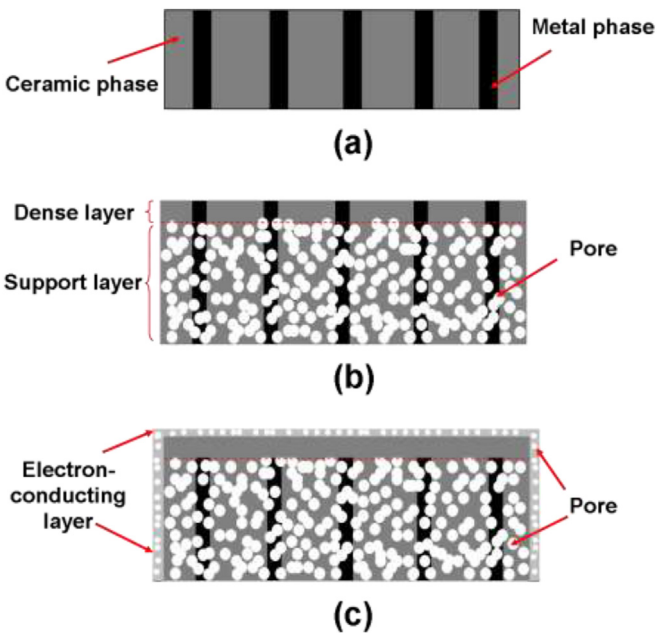

Fig. 1. Three configurations of hydrogen separation membrane based proton conductor. (a) Symmetric membrane; (b) asymmetric membrane; (c) ESC asymmetrical membrane.

membrane, the proton conductivity dominates hydrogen permeation because that the electron conductivity provided by Ni metal is far higher than proton conductivity from BZCY ceramic phase. This implies that increase of the proton conductivity of dense layer is the key to improve the hydrogen permeation. An intuitionistic strategy is to increase the volume of BZCY ceramic phase in dense layer.

In this work, the membrane configuration with asymmetrical structure and external short circuit (shown in Fig. 1c) in which nickel phase is instead of BZCY phase and the electron transportation can been performed by an external-circuit porous sliver coating layer, was designed to achieve the highest proton conductivity of dense membrane and meet the requirement of hydrogen permeation.

2. Experimental

$Ba(Zr_{0.1}Ce_{0.7}Y_{0.2})O_{3-\delta}$(BZCY) powders were synthesized via a citrate-nitrate combustion method. Initially, $BaCO_3$, $Ce(NO_3)_3$, $Y(NO_3)_3$ and $Zr(NO_3)_4$ were dissolved in distilled water in a stoichiometric ratio. Citric acid was added as a complexing agent, and the molar ratio of citric acid/metal ions was set to 6:4. Ammonia was used to adjust the pH value of the mixture to approximately 7. The solution was heated while stirring to evaporate water until it changed into a viscous gel. The gel was then ignited to by a flame and burned into in white ash. The obtained ash was calcined for 3 h at 1000 °C to remove carbon and form fine BZCY powders. The resulted BZCY, corn starch and NiO powders in weight ratio of 2:1:3 were well mixed by ball-milling with stabilized zirconia media in ethanol for 24 h and the final mixtures were used as the substrate powders.

A cost-saving dry-pressing method was employed to obtain a substrate-supported double-layer structure. Firstly, the substrate powders were pre-pressed under pressure of 200 MPa to form substrate. Secondly, loose BZCY powders were uniformly distributed over the substrate, co-pressed at 400 MPa and subsequently sintered at 1350 °C for 5 h to denitrify the BZCY membrane. At last, the sintered double-layer membrane was brushed Ag slurry on BZCY membrane surface and side, and calcined at 900 °C for 1 h in ambient air. The obtained sample was used as hydrogen permeation measurement.

The phase composition of the powders and membranes were identified by X-ray diffraction (XRD, Philips PW 1730 diffractometer) using Cu-Ka radiation. The surface and fracture morphology of the membrane was observed by a scanning electron microscope (SEM, JSM-6390LA). Hydrogen permeation measurements were conducted using a self-made device [12]. The membrane was sealed on alumina tube with a glass ring sealant at 990 °C for 15 min. Porous side of the asymmetric membrane was exposed to H_2/N_2 gas (with 3% H_2O). The other side was flushed with Ar at a flow rate of 20 mL/min. The components of the permeated gases on the sweep side were analyzed by a gas chromatograph (GC, Shimadzu GC-14C gas chromatograph). Hydrogen permeation through any incomplete seal was obtained by measuring the nitrogen concentration of the permeated gas.

3. Results and discussion

As shown in Fig. 2a, the as-prepared BZCY powders calcined at 1000 °C present the strong characteristic peaks of perovskite phase but a minor $BaCO_3$ peaks located at $2\theta = 24°$. The BZCY dense membrane sintered at 1350 °C exhibits a single perovskite phase structure without the appearance of other phases, indicating complete reaction of $BaCO_3$ (shown in Fig. 2b). Fig. 2c shows the XRD spectra of NiO-BZCY porous substrate. It could be clearly seen that there were only peaks corresponding to NiO and BZCY phase, which give evidence of good compatibility between BZCY and NiO.

The hydrogen permeation fluxes (JH_2) of Ni-BZCY symmetrical membrane, Ni-BZCY asymmetrical membrane and ESC asymmetrical membrane as a function of temperature in range from 700 to 900 °C are measured using dry argon as sweep gas with 20 ml min^{-1} flow rate and 20% H_2/N_2 (3%H_2O) as feed gas with 100 ml min^{-1} flow rate, as shown in Fig. 3a. It can be observed that JH_2 increases with the rising of temperature, because that the increasing of temperature increase the proton conductivity of BZCY ceramic phase. In investigated temperature range, hydrogen permeation fluxes of ESC asymmetrical membrane are higher than those of Ni-BZCY symmetrical membrane and asymmetrical membrane [7,11], which derived from thin electrolyte resistance and high membrane proton conductivity. Moreover, ESC

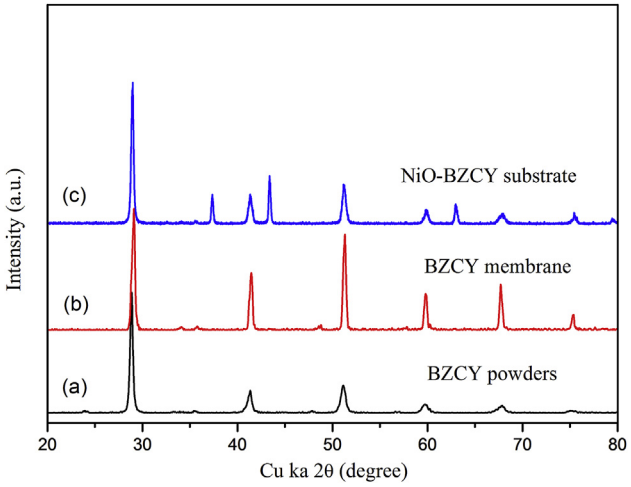

Fig. 2. X-ray diffraction patterns of (a) BZCY powders, (b) BZCY dense membrane surface and (c) porous NiO-BZCY substrate.

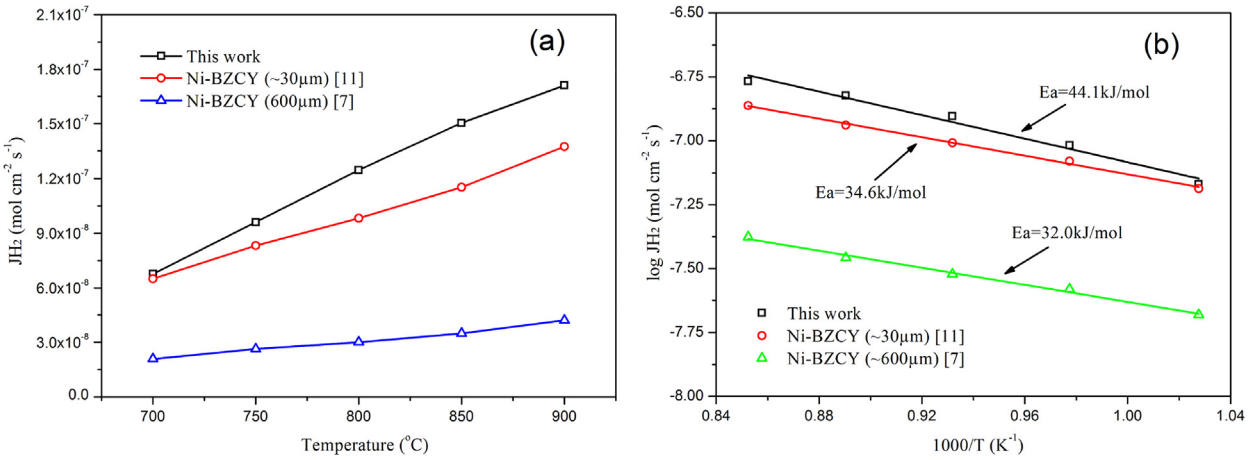

Fig. 3. Hydrogen permeation performance of BZCY-based hydrogen separation membranes with different configurations. (a) Temperature dependence of hydrogen fluxes; (b) Arrhenius plots of hydrogen fluxes.

asymmetrical membrane has a larger increase rate of hydrogen fluxes than Ni-BZCY membranes as the temperature increases from 700 to 900 °C. This maybe attributed to the difference of hydrogen permeation mechanism, membrane surface property and membrane configuration.

Fig. 3b shows the Arrheniius plots of hydrogen permeation fluxes for Ni-BZCY symmetrical membrane, Ni-BZCY asymmetrical membrane and ESC asymmetrical membrane. The activation energy (Ea) of hydrogen permeation can be calculated according to Arrhenius equation:

$$J(H_2) = A\exp\left(-\frac{Ea}{RT}\right), \tag{1}$$

where A and R are exponent factor and universal gas constant. Two Ni-BZCY membranes show nearly similar activation energy, 32.0 kJ/mol for Ni-BZCY asymmetrical membrane and 34.6 kJ/mol for Ni-BZCY asymmetrical membrane, suggesting that the same bulk diffusion mechanism and membrane surface property. However, the Ea of ESC asymmetrical membrane is 44.1 kJ/mol, obviously higher than those of Ni-BZCY membranes. Two main reasons maybe result in this difference. First, the hydrogen permeation mechanism is different. For ESC asymmetrical membrane the hydrogen permeation flux is determined by the proton transportation through BZCY ceramic phase, while for Ni-BZCY membrane hydrogen atom diffusion through nickel metal phase also contributed to the hydrogen permeation flux. Second, the distinct catalysis performance by surface Ag and Ni also leads to the difference of activation energy.

Hydrogen permeation fluxes as a function of hydrogen partial pressure gradient (ΔpH_2) at 850 °C are shown in Fig. 4. With increasing of ΔpH_2, the hydrogen fluxes increase from 1.45 to 2.17×10^{-7} mol cm^{-2} s^{-1}. Assuming that the hydrogen permeation through membrane is determined by ambipolar transport of protons and electrons and governed by bulk diffusion, the JH_2 will obey the Wagner equation:

$$J_{H_2} = \frac{RT}{4F^2L}\cdot\frac{\sigma_{H^+}\cdot\sigma_{el}}{\sigma_{H^+}+\sigma_{el}}\cdot\int_{p''_{H_2}}^{p'_{H_2}} d\ln pH_2, \tag{2}$$

where σ_{H^+} and σ_{el} respectively are proton and electron conductivity; $p'H_2$ and $p''H_2$ is the hydrogen partial pressure in the feed side and sweep side, respectively; L is the thickness of dense membrane; F is the Faraday constant; $\frac{\sigma_{H^+}\cdot\sigma_{el}}{\sigma_{H^+}+\sigma_{el}}$ is the ambipolar conductivity [13]. The

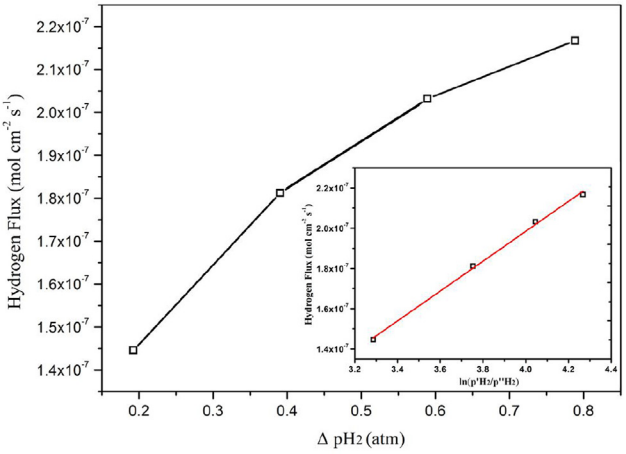

Fig. 4. Hydrogen fluxes function as hydrogen partial pressure gradient at 850 °C. The inset shows the relationship between JH_2 and.$\ln(p'H_2/p''H_2)$

inset in Fig. 4 presents the relationship JH_2 and $\ln(p'H_2/p''H_2)$. It is notable that the hydrogen flux is proportional to $\ln(p'H_2/p''H_2)$, indicating that the hydrogen transport occurred in accordance with the ambipolar diffusion mechanism in Eq. (2). It is obvious that the hydrogen permeation occurs via the ionic and electronic mixed

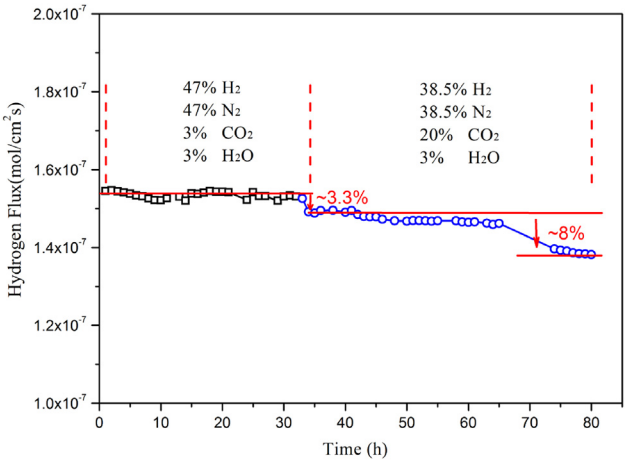

Fig. 5. The stability of hydrogen permeation through the ESC membrane.

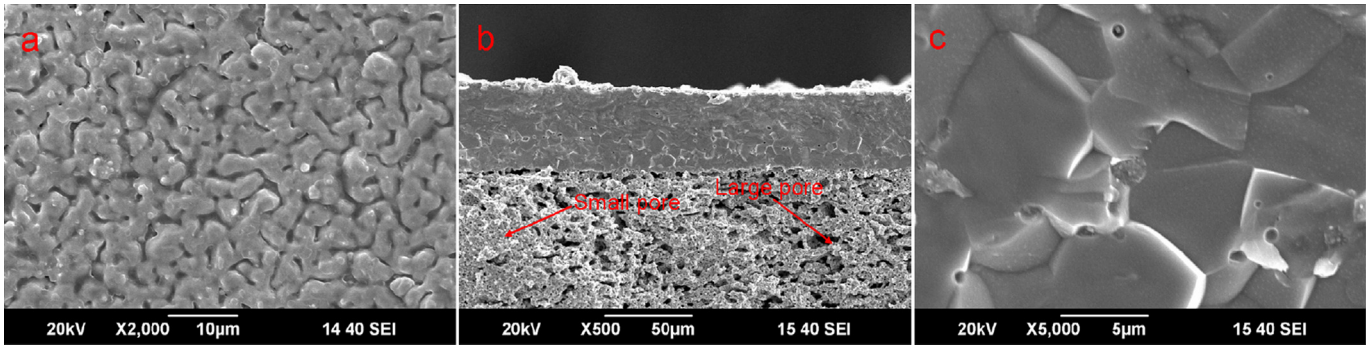

Fig. 6. Microstructure of ESC asymmetrical membrane after hydrogen permeation testing: (a) Surface of Ag-coating layer, (b) Fracture of ESC membrane, (c) Cross-section of BZCY dense layer.

conduction in ESC asymmetrical membrane. Meanwhile, this also demonstrates that the hydrogen permeation in ESC asymmetrical membrane is controlled by bulk diffusion of proton but not surface diffusion.

The stability of ESC membrane was investigated by the 80 h testing in 3% or 20% CO_2-containing atmosphere at 800 °C and the corresponding result was shown in Fig. 5. The hydrogen flux keeps stable in humid 3% CO_2-containing feed gas during 33-h testing. This attributes to the improvement of $BaCeO_3$ stability due to few Zr dopant [14]. When 20% CO_2 is added into the feed gas and the rate of feed gas remains constant, the hydrogen flux drops about 3.3%. The reason of the decreasing of hydrogen flux is that hydrogen partial pressure difference decrease, which decreases the driving force of hydrogen permeation. Hydrogen flux gradually decreases in 20% CO_2 atmosphere and after 50 h a decline of 8% can be seen. The reason is that BZCY is chemically unstable in high-contraction CO_2 atmosphere and reacts with CO_2 to form carbonate and oxide.

The microstructure of ESC membrane after testing was observed by SEM. Fig. 6a shows surface SEM image of Ag-coating layer. Some silver particles contact with each other and form porous network structure, which permit electron transportation in membrane surface. The proton reacts with electron to hydrogen on the triple-phase (proton conducting phase, electron conducting phase and gas phase) boundary. Moreover, Ag particles on surface are relatively large and the porosity is not high enough, which reduce the length of the triple-phase boundary. This attributes to high sealing temperature of 990 °C and therefore a sealant agent at lower temperature is indispensable in order to further improving hydrogen permeation performance. Fracture views of ESC membrane in Fig. 6b showed that the dense BZCY layer deposited onto the porous Ni-BZCY substrate and no distinct boundary between the two can be found, indicating a good thermal compatibility. The thickness of BZCY dense layer is ~45 μm and thin dense layer greatly reduced membrane resistance of proton conduction. Ag-coating layer is very thin so that it can not be evidently observed in cross-section morphology. The porous substrate contains small pores from nickel oxide reduction and large pores from starch combustion, which is beneficial for rapid transporting the gas onto internal surface of BZCY dense membrane. Magnified cross-section image of BZCY layer (Fig. 6c) confirmed that it is extremely dense except little close pores to prevent from gas leakage.

4. Conclusions

This work designs a new membrane configuration with asymmetrical structure and external short circuit for hydrogen separation, which provide a new method to improve the hydrogen permeation performance. The ESC asymmetrical membrane displays a high hydrogen permeation performance, 1.71×10^{-7} mol cm^{-2} s^{-1} at 900 °C using humidified 20% H_2/N_2 as feed gas and dry Ar gas as sweep gas. Hydrogen permeation flux increases with increasing of temperature and hydrogen partial pressure gradient. The relationship between JH_2 and $\ln(p'H_2/p''H_2)$ indicates that hydrogen permeation of the investigated ESC asymmetrical membrane occurs in accordance with the ambipolar diffusion mechanism and is controlled by the bulk diffusion. The durability of hydrogen flux in CO_2-containing atmosphere demonstrates that hydrogen permeation remains stable in low CO_2 concentration but became unstable in high CO_2 concentration.

Acknowledgment

This work is kindly supported by the National Natural Science Foundation of China (Grant No: 51408582).

References

[1] C.D. Zuo, S.E. Dorris, U. Balachandran, M.L. Liu, Effect of Zr-doping on the chemical stability and hydrogen permeation of the Ni–$BaCe_{0.8}Y_{0.2}O_{3-\alpha}$ mixed protonic-electronic conductor, Chem. Mater. 18 (2006) 4647–4650.
[2] S.J. Song, T.H. Lee, E.D. Wachsman, L. Chen, S.E. Dorris, U. Balachandran, Defect structure and transport properties of Ni–SrCeO3–δ cermet for hydrogen separation membrane, J. Electrochem. Soc. 152 (2005) J125–J129.
[3] W. Xing, G.E. Syvertsen, T. Grande, Z. Li, R. Haugsrud, Hydrogen permeation, transport properties and microstructure of Ca-doped $LaNbO_4$ and $LaNb_3O_9$ composites, J. Membr. Sci. 415–416 (2012) 878–885.
[4] Z.W. Zhu, W.P. Sun, Y.C. Dong, Z.T. Wang, Z. Shi, Q.P. Zhang, W. Liu, Evaluation of hydrogen permeation properties of Ni–$Ba(Zr_{0.7}Pr_{0.1}Y_{0.2})O_{3-\delta}$ cermet membranes, Int. J. Hydrog. Energy 39 (2014) 11683–11689.
[5] S.M. Fang, L. Bi, L.T. Yan, W.P. Sun, C.S. Chen, W. Liu, CO_2-resistant hydrogen permeation membranes based on doped ceria and nickel, J. Phys. Chem. C 114 (2010) 10986–10991.
[6] J. Yang, S.M. Fang, X.S. Wu, C.S. Chen, W. Liu, Hydrogen permeation of Ni–$BaCe_{0.9}Y_{0.1}O_{3-\delta}$ Cermet, J. Inorg. Mater. 22 (2007) 1243–1246.
[7] L.T. Yan, W.P. Sun, L. Bi, S.M. Fang, Z.T. Tao, W. Liu, Influence of fabrication process of Ni–$BaCe_{0.7}Zr_{0.1}Y_{0.2}O_{3-\delta}$ cermet on the hydrogen permeation performance, J. Alloy Compd. 508 (2010) L5–L8.
[8] G. Zhang, S. Dorris, U. Balachandran, M. Liu, Effect of Pd Coating on hydrogen permeation of Ni–barium cerate mixed conductor, Electrochem. Solid-State Lett. 5 (2002) J5–J7.
[9] S.J. Song, J. Moon, T. Lee, S. Dorris, U. Balachandran, Thickness dependence of hydrogen permeability for Ni–$BaCe_{0.8}Y_{0.2}O_{3-\delta}$, Solid State Ion. 179 (2008) 1854–1857.
[10] C.D. Zuo, T.H. Lee, S.E. Dorris, U. Balachandran, M.L. Liu, Composite Ni–Ba(Zr0.1Ce0.7Y0.2)O3 membrane for hydrogen separation, J. Power Sources 159 (2006) 1291–1295.
[11] Z.W. Zhu, W.P. Sun, L.T. Yan, W.F. Liu, W. Liu, Synthesis and hydrogen permeation of Ni–$Ba(Zr_{0.1}Ce_{0.7}Y_{0.2})O_{3-\delta}$ metal–ceramic asymmetric membranes, Int. J. Hydrog. Energy. 36 (2011) 6337–6342.
[12] Z.W. Zhu, W.P. Sun, Z.T. Wang, J.F. Cao, Y.C. Dong, W. Liu, A high stability Ni–$La_{0.5}Ce_{0.5}O_{2-\delta}$ asymmetrical metal-ceramic membrane for hydrogen separation and generation, J. Power Sources 281 (2015) 417–424.
[13] T. Norby, Y. Lerring, Mixed hydrogen ion–electronic conductors for hydrogen permeable membranes, Solid State Ion. 136–137 (2000) 139–148.
[14] C.D. Zuo, S.W. Zha, M.L. Liu, M. Hatano, M. Uchiyama, $Ba(Zr_{0.1}Ce_{0.7}Y_{0.2})O_{3-d}$ as an electrolyte for low-temperature solid-oxide fuel cells, Adv. Mater. 18 (2006) 3318–3320.